PNAS
www.pnas.org

Supplementary Information for

Label-free chemical imaging flow cytometry by high-speed multicolor stimulated Raman scattering

Yuta Suzuki, Koya Kobayashi, Yoshifumi Wakisaka, Dinghuan Deng, Shunji Tanaka, Chun-Jung Huang, Cheng Lei, Chia-Wei Sun, Hanqin Liu, Yasuhiro Fujiwaki, Sangwook Lee, Akihiro Isozaki, Yusuke Kasai, Takeshi Hayakawa, Shinya Sakuma, Fumihito Arai, Kenichi Koizumi, Hiroshi Tezuka, Mary Inaba, Kei Hiraki, Takuro Ito, Misa Hase, Satoshi Matsusaka, Kiyotaka Shiba, Kanako Suga, Masako Nishikawa, Masahiro Jona, Yutaka Yatomi, YalikunYaxiaer, Yo Tanaka, Takeaki Sugimura, Nao Nitta, Keisuke Goda, and Yasuyuki Ozeki

Yasuyuki Ozeki
Email: ozeki@ee.t.u-tokyo.ac.jp

This PDF file includes:

Supplementary text
Figs. S1 to S5

www.pnas.org/cgi/doi/10.1073/pnas.1902322116

Supplementary Information Text

SRS spectral analysis of *E. gracilis* cells. To precisely obtain the SRS spectra of chemical constituents in *E. gracilis* cells including lipid droplets and paramylon particles whose size are on the order of several micrometers, we separately measured them while flowing the cells at a much slower flow rate than 2 cm/s (i.e., the flow rate in the experiments presented in Figs. 2, 3, and 4). Specifically, we initially injected a cell sample into the microfluidic device at 2 cm/s using a syringe pump and then stopped the injection by turning off the pump. After stopping the injection, we recorded the images of the cells while the cellular flow speed was gradually slowing down. One representative four-color SRS image of a *E. gracilis* cell is shown in Fig. S2 *A*. Since we are uncertain of what the flow rate of the cells was when we captured the image, the shown scale bar is applicable only in the image's horizontal direction. The extracted four-color spectra at the three locations indicated by the arrows in the figure is plotted in Fig. S2 *B*, together with the 91-color spectra acquired by our SRS microscope by sweeping the vibrational frequency from 2800 cm^{-1} to 3100 cm^{-1} using fixed *E. gracilis* cells. We note that both four-color and 91-color spectra are normalized by summed values of SRS signal intensity at 2860, 2910, 2937, and 3040 cm^{-1} of each spectrum. The plot shows significant overlap between the 4- and 91-color SRS spectra, demonstrating our SRS flow cytometer's capability to acquire highly reliable SRS spectral images of *E. gracilis* cells. Using these extracted four-color spectra, we performed linear decomposition on the four-color SRS images, whose result is shown in Fig. S2 *C*. In the figure, we clearly see the distinct spatial distribution of the intracellular concentrations of paramylon, chlorophyll, and lipids, showing the system's chemical imaging capability.

SRS spectral analysis of blood cells. To generate multicolor SRS images of blood cells and cancer cells shown in Fig. 4 from raw four-color SRS images shown in Fig. S3 *A*, we used spectral bases shown in Fig. S3 *B*, which were manually extracted from raw SRS images. Since we used different spectral bases for different types of cells, we did not directly compare the multicolor images between different cell types. The colors of cell images shown in Fig. 4 are only for the purpose of visualization. In turn, the CNN analysis was conducted using raw four-color SRS images instead of decomposed images so that direct comparison and classification between different cell types were achieved.

Scatter plots of blood cells. Fig. S4 shows the scatter plots of cell area and four-color SRS signals integrated over the cell area, indicating features for each cell type. For example, the differences between whole blood cells, PBMCs, Jurkat cells, and HT29 cells are relatively apparent in the plot of cell area and $\lambda 1$ intensity; Jurkat cells and HT29 cells have larger area than whole blood cells and PBMCs, and whole blood cells and HT29 cells exhibit higher $\lambda 1$ intensity than PBMCs and Jurkat cells. Nevertheless, there is a significant overlap between all the cell types in all the plots. In contrast, the CNN gives excellent classification accuracy as shown in Fig. 4*C*, demonstrating the effectiveness of image-based classification.

Noise measurement. To confirm that the noise level of our SRS detection system is shot-noise-limited, we measured the DC signal of the SRS photodetector and the variance of our lock-in amplifier signal with an oscilloscope by changing the optical power at the photodetector. As shown in Fig. S5, both the DC signal and the variance changed linearly, provided that the optical power was less than 80 mW, indicating that the Ti:sapphire laser pulses were shot-noise-limited. The variance without any optical input (i.e., 10 mV^2) corresponds to the circuit noise. At an optical power of 60 mW, which was the typical value used in our experiments, the total noise level is 42 mV^2, which is the sum of the circuit noise (10 mV^2) and the shot noise (32 mV^2). Thus, the circuit noise is ~5 dB less than the shot noise in the experiments.

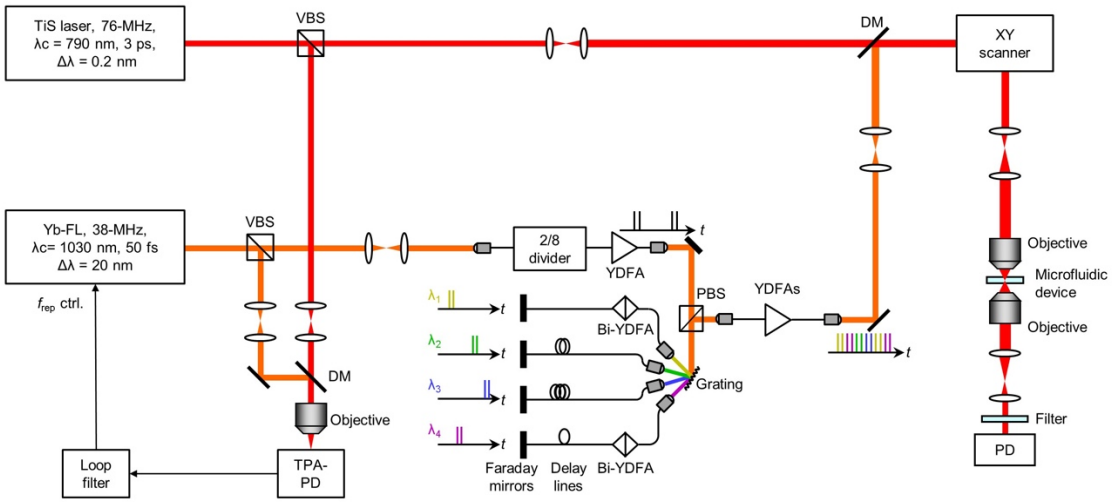

Fig. S1. Detailed schematic of the SRS imaging flow cytometer. VBS: variable beam splitter composed of a half-wave plate and a PBS; TPA-PD: two-photon absorption photodiode; DM: dichroic mirror; YDFA: polarization-maintaining Yb-doped fiber amplifier; Bi-YDFA: bidirectional polarization-maintaining Yb-doped fiber amplifier; PBS: polarizing beam splitter; PD: photodiode.

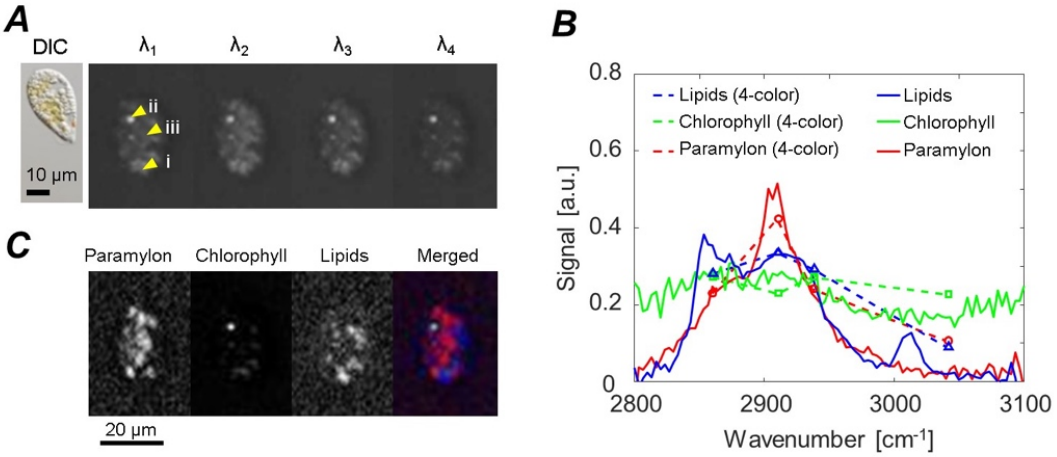

Fig. S2. Extraction of SRS spectra from *E. gracilis* cells in SRS imaging flow cytometry. (*A*) Raw four-color images of a *E. gracilis* cell. (*B*) Four-color SRS spectra of three chemical constituents inside *E. gracilis* cells (lipids, chlorophyll, and paramylon, extracted from pixel locations i-iii shown in (*A*), respectively) overlaid with the spectra obtained by continuously scanning the Raman frequency between 2800 and 3100 cm^{-1}, using a fixed sample. (*C*) Chemically decomposed images of the three constituents of a *E. gracilis* cell. Red, green, and blue parts in the merged image indicate paramylon, chlorophyll, and lipids, respectively.

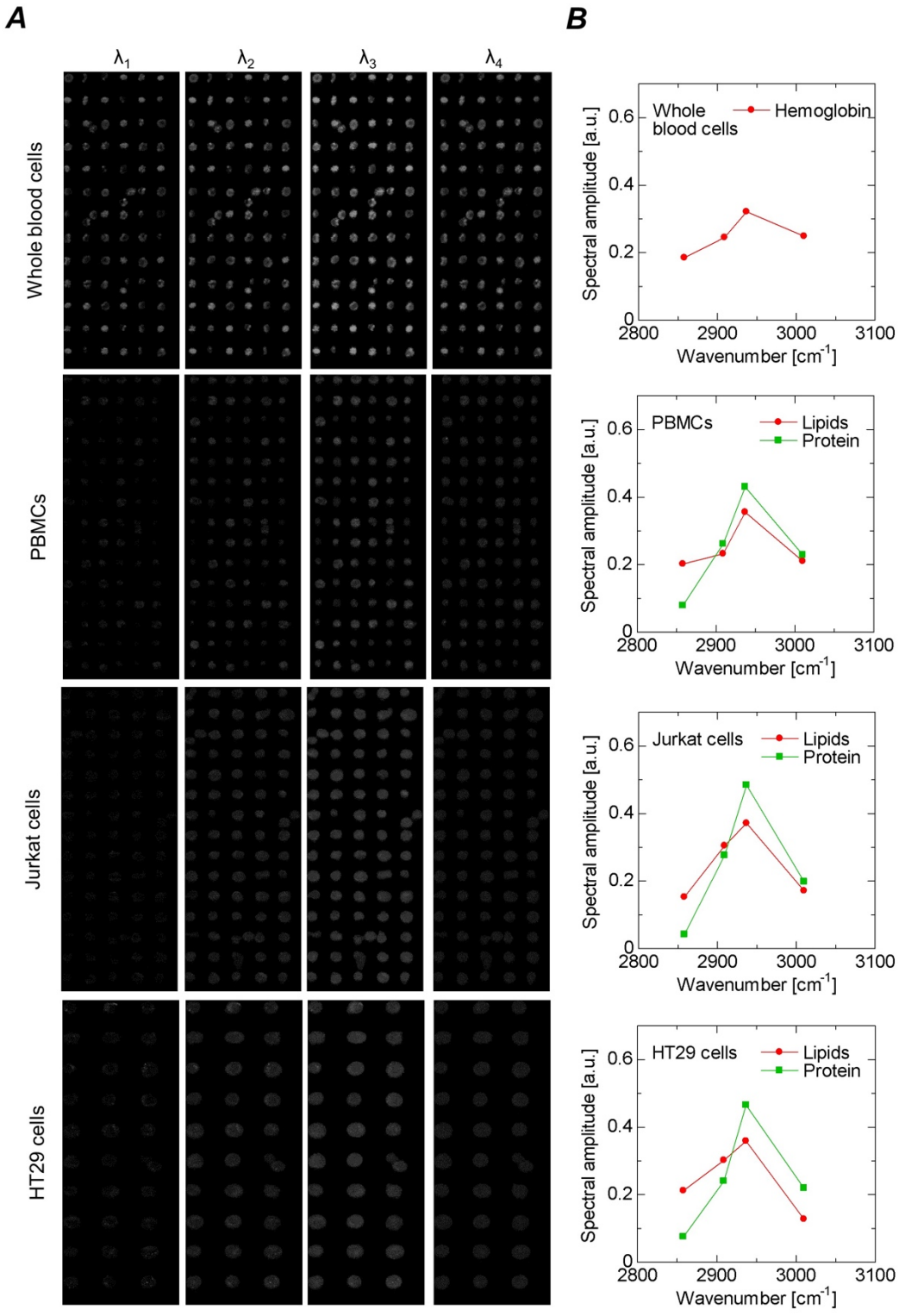

Fig. S3. Raw four-color SRS images and spectral bases of whole blood cells, PBMCs, Jurkat cells, and HT29 cells. (*A*) Image library of four-color SRS images. (*B*) Spectral bases used in the image decomposition for multicolor imaging.

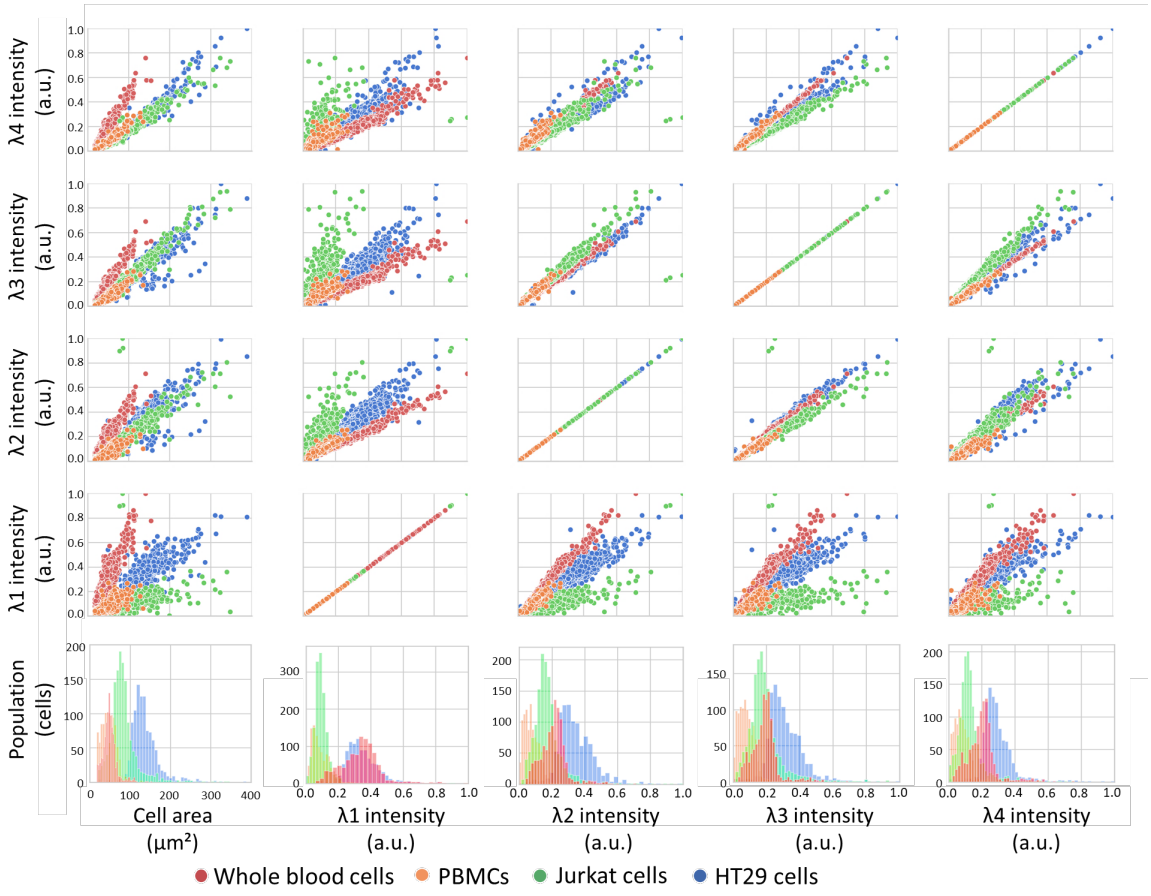

Fig. S4. Scatter plots and histograms of Jurkat cells, HT29 cells, PBMCs, and whole blood cells in cell area and four-color SRS signal intensities. λ_1: 2858 cm^{-1}; λ_2: 2909 cm^{-1}; λ_3: 2937 cm^{-1}; λ_4: 3010 cm^{-1}.

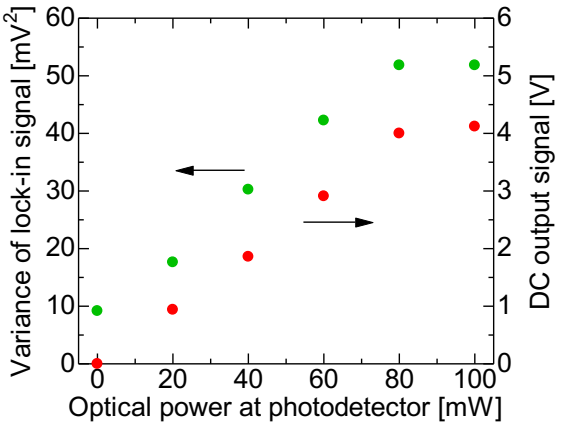

Fig. S5. Evaluation of the linearity and noise level of our SRS photodetector and lock-in amplifier. The green and red circles show the variance of the output signal of our home-made lock-in amplifier (left axis) and the DC output signal of the SRS photodetector (right axis), respectively, at several optical power values of the Ti:sapphire laser pulses at the PD. The PD response is linear to the input optical power up to 80 mW.